International Journal of Nanomedicine Dovepress

Open Access Full Text Article ORIGINAL RESEARCH

Development of the Curcumin Analog CA7 Liposome and Its Evaluation for Efficacy Against Cervical Cancer in vitro and in vivo

Linjin Xiong[1–4,*], Yumeng Wei[1,3,*], Hui Si[4,*], Zheng Li[1–3], Jie Wen[1–3], Furong Liu[5], Xiaodong Wang[6], Hongru Yang[7], Ligang Chen[8], Chao Pi[1,3], Yunwei Han[7], Ling Zhao[2–4]

[1]Key Laboratory of Medical Electrophysiology, Ministry of Education, School of Pharmacy of Southwest Medical University, Luzhou, 646000, People's Republic of China; [2]Department of Psychiatry, Fundamental and Clinical Research on Mental Disorders Key Laboratory of Luzhou, The Affiliated Hospital, Southwest Medical University, Luzhou, Sichuan, 646000, People's Republic of China; [3]Central Nervous System Drug Key Laboratory of Sichuan Province, School of Pharmacy, Southwest Medical University, Luzhou, Sichuan, 646000, People's Republic of China; [4]Luzhou Key Laboratory of Traditional Chinese Medicine for Chronic Diseases Jointly Built by Sichuan and Chongqing, The Affiliated Traditional Chinese Medicine Hospital, Southwest Medical University, Luzhou, Sichuan, 646000, People's Republic of China; [5]Department of Oncology, The Affiliated Traditional Chinese Medicine Hospital, Southwest Medical University, Luzhou, Sichuan, 646000, People's Republic of China; [6]Department of Hepatobiliary Diseases, The Affiliated Traditional Chinese Medicine Hospital, Southwest Medical University, Luzhou, Sichuan, 646000, People's Republic of China; [7]Department of Oncology, The Affiliated Hospital of Southwest Medical University, Luzhou, Sichuan, 646000, People's Republic of China; [8]Department of Neurosurgery, The Affiliated Hospital of Southwest Medical University, Luzhou, Sichuan, 646000, People's Republic of China

*These authors contributed equally to this work

Correspondence: Chao Pi, Central Nervous System Drug Key Laboratory of Sichuan Province, School of Pharmacy of Southwest Medical University, No. 1, Section 1, Xianglin Road, Longmatan District, Luzhou, Sichuan, 646000, People's Republic of China, Tel/Fax: +86 830 3162291, Email pichao2016@163.com; Ling Zhao, Department of Psychiatry, Fundamental and Clinical Research on Mental Disorders Key Laboratory of Luzhou, The Affiliated Hospital, Southwest Medical University, Luzhou, Sichuan, 646000, People's Republic of China, Tel/Fax +86 830 2681630, Email zhaoling@swmu.edu.cn

Objective: The objective of this study was to develop liposomes (LP) containing a curcumin (CU) analog CA7 to enhance its pharmacokinetic profile and anti-cervical cancer (CC) effects.

Methods: Single-factor and Box-Behnken experiments were conducted to optimize the formulation of CA7-loaded liposomes (CA7-LP). The in vitro release, stability, biocompatibility, and pharmacokinetic of CA7-LP were evaluated. The biological effects of CA7-LP on Hela cells were assessed using MTT assays, colony formation assays, wound healing assays, and flow cytometry. Additionally, the anti-CC efficacy of CA7-LP was tested in mouse models of transplanted tumors.

Results: The optimal formulation of CA7-LP exhibited a particle size of 92.43 ± 1.52 nm, a polydispersity index of 0.27 ± 0.01, an encapsulation efficiency of 97.79 ± 1.49%, a drug loading of 3.23 ± 0.20%, and a zeta potential of −6.69 ± 0.77 mV. Transmission electron microscopy confirmed that a spherical morphology was exhibited by CA7-LP. The cumulative in vitro release of CA7-LP was found to be 2.84 times greater than that of CA7, and stability at room temperature was maintained for at least 90 d. Furthermore, a significantly higher uptake of CA7-LP by Hela cells was observed compared to curcumin and CA7, leading to enhanced inhibition of cell proliferation, migration and cell cycle, as well as increased apoptosis ($p < 0.05$). In vivo studies revealed that CA7-LP exhibited superior pharmacokinetic properties compared to CA7 (AUC: 3.58-fold, C_{max}: 5.65-fold, $t_{1/2z}$: 1.2-fold). The anti-CC effects of CA7-LP were found to be comparable to those of Cisplatin injection, with a better safety profile.

Conclusion: The newly developed CA7-LP is considered a promising candidate for the treatment of CC, demonstrating high potential for clinical application.

Keywords: curcumin analog CA7, liposome, cervical cancer, hela

Introduction

Cervical cancer (CC) is one of the most common causes of cancer-related deaths among women worldwide. In 2022, there were an estimated 661,021 new cases and 348,189 deaths attributed to CC globally.[1–3] While the availability of

Received: 26 August 2024
Accepted: 26 November 2024
Published: 13 December 2024

Graphical Abstract

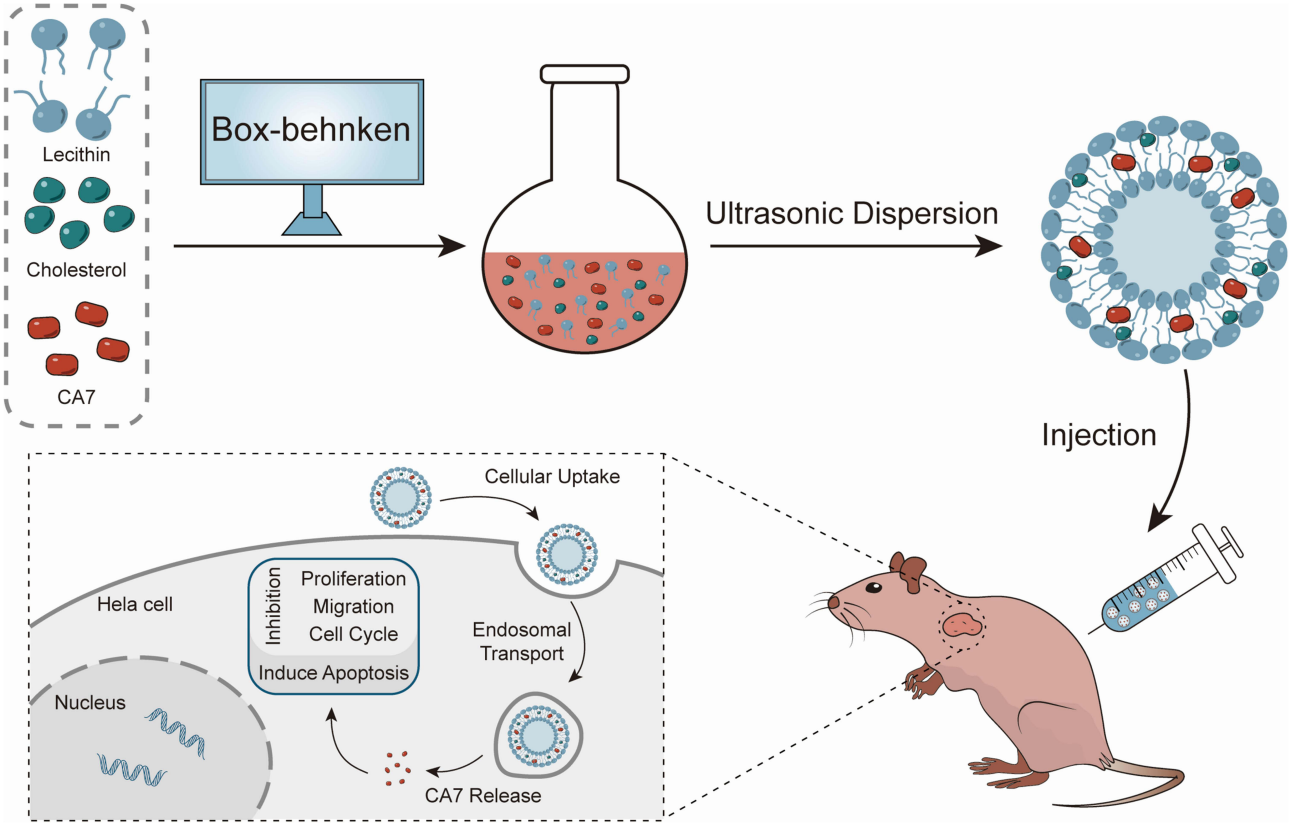

HPV vaccines has helped reduce the incidence of CC, large-scale HPV vaccination campaigns face significant challenges, particularly in economically disadvantaged regions, thereby maintaining CC as a pressing public health concern.[4,5] Chemotherapy remains a standard treatment for advanced and recurrent CC, with platinum-based drugs like Cisplatin injection (DDP-INJ) being commonly used in concurrent chemoradiotherapy for locally advanced cases.[6] However, the toxic side effects associated with DDP, such as gastrointestinal issues and renal impairment, often lead to poor patient outcomes.[6,7] Consequently, there is an urgent need to develop safe and effective new agents against CC.

In recent years, the exploration of natural products for anti-cancer drug development has gained traction. Curcumin (CU), a natural compound extracted from the rhizomes of turmeric, has demonstrated various pharmacological activities, including anti-tumor, anti-oxidant, anti-inflammatory, and anti-microbial effects.[8–12] Notably, CU has exhibited a favorable safety profile, with single oral doses of up to 12 g being well tolerated.[13] Of particular interest, research has shown that CU can prevent and treat CC through multiple mechanisms, such as inhibiting HPV replication and triggering apoptosis and autophagy while preventing cancer cell proliferation, migration, and invasion.[14–16] However, the clinical application of CU is significantly limited by its poor water solubility (approximately 0.125mg/L) and low bioavailability.[17–19]

To address the limitations of CU in anti-cancer therapies, researchers have developed various CU analogues that demonstrate improved physicochemical properties and anti-cancer activities.[20–27] For example, asymmetric monocarbonyl analogs fused with 1-aryl-1H-pyrazole have been shown to alter the morphology of breast cancer cells and enhance caspase-3 activity, promoting cell death.[28] Another analogue, (2E,6E)-2,6-bis(2,3-dimethoxybenzylidene)cyclohexanone, has improved bioavailability of CU and significantly induced apoptosis in colorectal cancer cells.[29] These findings suggest that developing CU analogues is a promising strategy to overcome the inherent limitations of CU. In our previous

study, a series of CU analogues were designed, synthesized, and screened, with CA7 emerging as a new analogue that exhibits significant anti-CC effects and improved water solubility (approximately 32.9 mg/L).[30] Despite these advancements, CA7 still faces challenges related to solubility and bioavailability, highlighting the need for a nano delivery system to enhance its pharmacological properties.

In the realm of nanomedicine, liposomes (LP) represent one of the earliest forms of clinical applications and have been extensively utilized in cancer treatment.[31,32] LP serve as an ideal platform for delivering chemotherapy drug due to their high biocompatibility, enhanced drug efficacy, increased bioavailability, and reduced toxicity.[31–33] Particularly, a nano delivery system that incorporates CU into LP, modified with specific peptides, has shown improved targeting of solid tumors and enhanced solubility for CU.[34] Additionally, LP delivery systems loaded with poorly soluble drugs like Paclitaxel have demonstrated enhanced anti-tumor efficacy.[35] Therefore, LP is currently recognized as the most promising drug delivery system for cancer therapy.

In this study, the LP delivery system for CA7 (CA7-LP) was developed to enhance the druggability of CA7 for the first time. The effects of CA7-LP on Hela cell proliferation, migration, cell cycle, and apoptosis were evaluated. Furthermore, the pharmacokinetics, biosafety, and anti-CC efficacy of CA7-LP were assessed in vivo, aiming to provide experimental and theoretical basis for the development of new anti-CC drugs.

Materials and Methods

Chemicals and Reagents

CU (purity ≥ 99%) was purchased from Chengdu Best Reagent Co., Ltd. CA7 (purity ≥ 99%) was independently synthesized by the Pharmaceutical Laboratory team at Southwest Medical University (Figure 1). Lecithin were purchased from Shanghai Aladdin Bio-Chem Technology Co., Ltd. Cholesterol was purchased from Shanghai Macklin Bio-Tech Co., Ltd. MTT, Hoechst 33258, penicillin-streptomycin-amphotericin B, trypsin-EDTA (0.25%), crystal violet staining solution, and cell cycle/apoptosis detection kits were all purchased from Beyotime Biotechnology Co., Ltd. Dulbecco's Modified Eagle Medium (DMEM), dimethyl sulfoxide (DMSO), and heat-inactivated fetal bovine serum (FBS) were

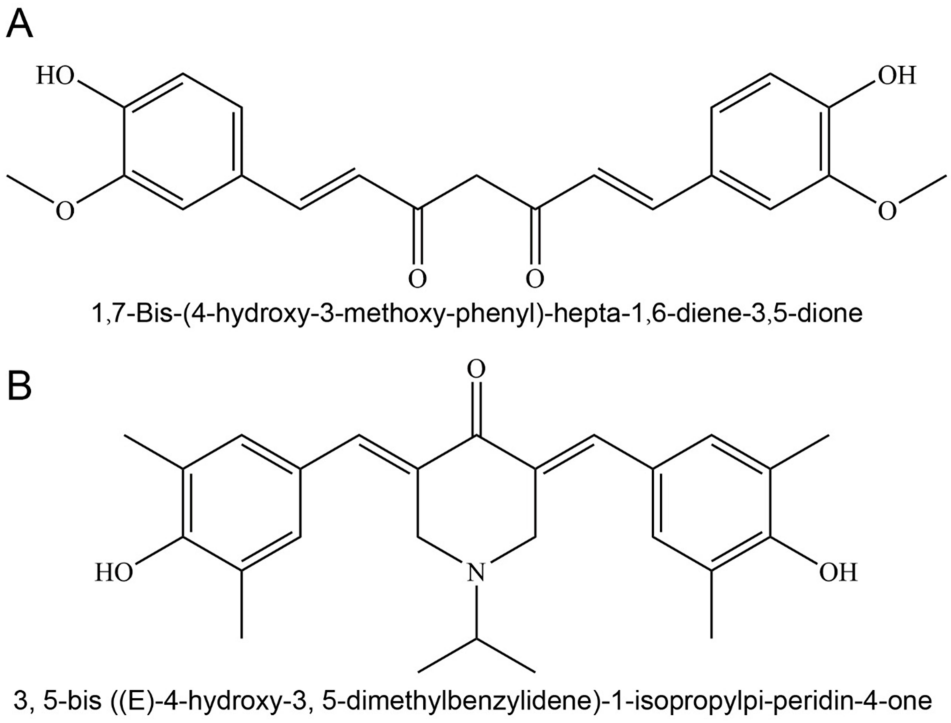

Figure 1 Chemical structure of CU (**A**) and CA7 (**B**).

purchased from Beijing Thermo Fisher Scientific Co., Ltd. Annexin V-FITC/PI dual-staining apoptosis detection kit was purchased from Jiangsu KeyGEN Biological Technology Co., Ltd.

Cell Lines and Animals

Hela cells were obtained from the Cell Bank Center of the Chinese Academy of Sciences. These cells were cultured in DMEM supplemented with 10% FBS and 1% penicillin-streptomycin-amphotericin B, and incubated at 37°C with 5% CO_2 in an incubator. The cell culture medium was replaced with fresh DMEM every 2 d. When the cells reached 80–90% confluence, they were detached using trypsin-EDTA (0.25%).

Female SD rats were purchased from the Animal Experimental Center of Southwest Medical University (License: SYXK (Chuan) 2023-0065). BALB/c immunodeficient mice (female, 4 w, 15–16 g) were purchased from Beijing Huafukang Biotechnology Co., Ltd (License: SCXK (Beijing) 2019-0008). The Animal Experimental Ethics Committee of Southwest Medical University in Luzhou, People's Republic of China, approved the animal care and handling protocols for this study.

Construction and Optimization of CA7-LP

CA7-LP was prepared using an ultrasonic dispersion technique. Briefly, CA7, lecithin, and cholesterol were dissolved in 6 mL of methanol and dried with a rotary evaporator set at 150 rpm. The residual solvent was then removed in a vacuum drying oven at 37°C for 3 h. The resulting lipid film was hydrated with distilled water and subjected to probe sonication at 160 W for 4 min to obtain CA7-LP. Sucrose (3% w/v) was chosen as the lyoprotectant, and the mixture was freeze-dried for 24 h using a freeze dryer (LGJ-18C, Beijing Sihuan Scientific Instrument Factory Co., Ltd.), yielding CA7-LP in powdered form.

Based on the results of single-factor experiments, the Box-Behnken design (BBD) was employed using Design Expert 8.0.2 software to optimize the formulation of CA7-LP and obtain the optimal product. CA7 dosage (X_1), lecithin dosage (X_2) and cholesterol dosage (X_3) were chosen as variables (Table S1), while particle size (PS), polydispersity index (PDI), and encapsulation efficiency (EE) were selected as response variables.

HPLC Analysis

Quantitative analysis was performed using the Agilent 1260 HPLC system. The separation was carried out on a Phenomenex Luna® 5 µm C18(2) 100 Å LC column (250 × 4.6 mm). The detection wavelength was set at 397 nm, and the column temperature was maintained at 30°C. A mobile phase consisting of 0.1% phosphoric acid solution and methanol (35:65, v/v) was used for elution at a flow rate of 0.8 mL/min.

Characterization of CA7-LP

Evaluation of Encapsulation Efficiency and Drug Loading

Due to the strong lipophilicity of CA7, the unencapsulated CA7 not incorporated into the LP tends to precipitate and separate during low-speed centrifugation. To determine the EE, 0.1 mL of CA7-LP supernatant after centrifugation at 8000 rpm for 10 min was taken and dissolved in 4 mL of methanol. The amount of encapsulated drug (W_e) is then measured using a HPLC system according to a pre-established analytical method. The total drug mass (W_t) is assessed using an equivalent volume of the non-centrifuged CA7-LP suspension.

For drug loading (DL) assessment, a precise amount of the freeze-dried CA7-LP powder (W_N) is weighed and dissolved in a suitable volume of methanol. Following sonication and centrifugation (8000 rpm, 10 min), the supernatant is collected to measure W_t.

The formulas for calculating EE% and DL% are as follows:

$$EE\% = (W_e/W_t) \times 100\%$$

$$DL\% = (W_t/W_N) \times 100\%$$

W_e represents the mass of the drug encapsulated in the LP, W_t represents the total mass of the drug in the CA7-LP suspension or lyophilized powder, and W_N represents the total mass of the LP (including both the drug and excipients).

Determination of PS, PDI, Zeta Potential and Morphological Observation

The PS, PDI, and zeta potential of CA7-LP were measured using the Malvern Zetasizer Nano series-ZS (Malvern Instruments, Malvern, Worcestershire, UK). The sample was diluted 1:20 with distilled water and measured at room temperature. Samples for zeta potential measurements were placed in specialized cuvettes capable of conducting current during analysis. The electrophoretic mobility (μm/s) was then converted to zeta potential using built-in software, based on the Helmholtz-Smoluchowski equation. A diluted solution of CA7-LP in distilled water was applied to a nitrocellulose-coated copper grid, followed by staining with 2% phosphotungstic acid. After drying, the samples were imaged using transmission electron microscopy.

Stability Studies

According to the optimized formulation and process, both the CA7-LP suspension and freeze-dried powder were prepared and stored at 25 ± 2°C and 4 ± 2°C, respectively. The PS, PDI, and EE of CA7-LP were measured at various time points.

Evaluation of Drug Release in vitro

To evaluate the release kinetics of CA7-LP in vitro, equal volumes of CA7 methanol solution and CA7-LP (both at the same concentration) were added to dialysis bags (8000–14000 Da) and placed in 150 mL of phosphate-buffered saline (PBS) containing 0.35% (v/v) Tween 80. The system was maintained at 37°C with gentle stirring at 100 rpm. At predetermined intervals, samples were taken for analysis, and an equal volume of blank media was replenished.

Biocompatibility Evaluation

To evaluate biocompatibility, blood was collected from healthy rats and stirred continuously in the same direction for 6 min to destroy fibrinogen. The blood was then diluted with saline and centrifuged at 1500 rpm for 10 min to remove the supernatant. This washing process was repeated until the supernatant became clear, leaving a purified red blood cells (RBCs). The RBCs were then prepared as a 2% RBC saline suspension.

For the hemolysis test, the RBCs suspension (2%) was mixed with saline, ultrapure water, or CA7-LP at different concentrations, as outlined in Table S2. Samples 1–6 contained varying concentrations of CA7-LP, while samples 7 and 8 served as negative and positive controls, respectively. After incubation at 37°C for 5 h, the OD value of each sample was measured at 540 nm using a microplate reader (Spectra Max M3, Molecular Devices, USA). The hemolysis rate (%) was calculated for each group to determine the biocompatibility of CA7-LP.

$$\text{Hemolysis rate}\,(\%) = \left(OD_{sample} - OD_{negative}\right) / \left(OD_{positive} - OD_{negative}\right) \times 100\%$$

Cell Viability Assay

Hela cells (4.5×10^3 cells/well) were inoculated in a 96-well plate and allowed to adhere for 24 h. The cells were treated with gradient concentrations of CU, CA7, CA7-LP, and DDP for 24, 48, and 72 h. DMSO (0.1%) served as a negative control. To assess cell viability, 20 μL of freshly prepared MTT solution was added to each well, followed by incubation at 37°C for 3.5 h. After removing the culture medium, 150 μL of DMSO was added to dissolve the formazan crystals. The OD values were measured at 490 nm using a microplate reader (Spectra Max M3, Molecular Devices, USA), and the cell inhibition rate was calculated.

$$\text{Inhibition rate}\,(\%) = \left[1 - \left(OD_{sample} - OD_{blank}\right) / \left(OD_{control} - OD_{blank}\right)\right] \times 100\%$$

Colony Formation Assay

Hela cells were seeded at a density of 1×10^3 cells per well in a 6-well plate. Different concentrations of CU, CA7, CA7-LP, and DDP were prepared in the DMEM, and the Hela cells were intervened for 6 h. Afterward, fresh medium was

continued to incubate for 7 d. Following incubation, the cells were fixed with 4% paraformaldehyde for 12 min and stained with crystal violet for 60 min. Representative images were captured using an inverted microscope (TS2R-LS, Nikon, Japan) to visualize colony formation.

Wound Healing Assay

Hela cells (9×10^5 cells/well) were seeded in a 6-well plate. Once the cell monolayer formed, a wound was created by scraping vertically with a 200 μL pipette tip. The cells were washed twice with PBS, and different concentrations of CU, CA7, CA7-LP, and DDP in serum-free DMEM were added to the respective wells. The plates were then incubated at 37°C with 5% CO_2. The migration of cells was monitored under a microscope (TS2R-LS, Nikon, Japan) at 0 h and 24 h to observe the wound closure.

Cell Apoptosis Detection

Hela cells (5.5×10^5 cells/well) were seeded in a 6-well plate and treated with different concentrations of CU, CA7, CA7-LP, and DDP in DMEM for 24 h. For flow cytometry analysis, the aforementioned Hela cells were collected and resuspended in 250 μL of Binding Buffer, and gently pipetted to form a single-cell suspension. Annexin V-FITC (5 μL) and PI (5 μL) were added sequentially to the suspension and incubated in the dark for 10 min at room temperature. Apoptosis was analyzed using a flow cytometer (FACSAriaIII, BD, USA).

Cell Cycle Assay

Hela cells (5.5×10^5 cells/well) were inoculated in a 6-well plate and treated with different concentrations of CU, CA7, CA7-LP, and DDP in DMEM for 24 h. Following the manufacturer's instructions, 70% ethanol was slowly added dropwise into the collected cells. The cells were then stored at −20°C for 24 h. After washing twice with pre-chilled PBS, the cells were stained with PI staining buffer in the dark for 30 min at room temperature. Cell cycle distribution was then analyzed by flow cytometer (FACSAriaIII, BD, USA).

Cellular Uptake Experiments

The intrinsic fluorescence of CU and CA7 allowed for direct observation of drug distribution within cells using laser confocal microscopy. In brief, Hela cells were seeded in a 24-well plate with sterile glass coverslips. After cell adhesion, they were treated with DMEM containing 7.5 μM of CU, CA7, and CA7-LP for 24 h. The cells were then fixed with 4% paraformaldehyde and stained with Dil staining solution. Cellular uptake was observed using a laser confocal microscope (LSM980, Zeiss, Germany).

Pharmacokinetic Studies

Ten female SD rats (180 ± 20 g) were obtained from the Experimental Animal Center of Southwest Medical University. After a 7-day acclimation period, the rats were fasted for 12 h before the experiment and randomly divided into two groups. Both CA7 and CA7-LP were administered via the tail vein at a dose of 20 mg/kg. CA7 was dissolved in a solvent mixture of ethanol and polyethylene glycol hydrogenated castor oil (1:1, v/v), while CA7-LP was dissolved in saline with the aid of ultrasound. Blood samples were collected at intervals of 3, 5, 10, 15, 30, 60, 120, 240, and 480 min post-administration and centrifuged (6000 rpm, 3 min) to collect the plasma for HPLC analysis.

In vivo Anti-Tumor Effect Studies

Hela cells (3.5×10^7 cells) were suspended in 100 μL of PBS and subcutaneously injected near the right scapula of nude mice. When tumor volumes reached approximately 100 mm^3, the mice were randomly assigned to five groups (n = 5): (1) Saline (control), (2) CU (50 mg/kg), (3) CA7 (50 mg/kg), (4) CA7-LP (50 mg/kg), and (5) DDP-INJ (3.5 mg/kg). The treatments were administered intraperitoneally every 2 days for 14 days. Tumor volume ($V = 1/2 * ab^2$, where a is the long axis and b is the short axis) and body weight were recorded throughout the study. After treatment, the nude mice were sacrificed, and the tumors were excised and weighed. Subsequently, the hearts, livers, lungs, kidneys, and tumors of the nude mice were then fixed in 10% formalin and embedded in paraffin for histological sectioning. The sections of the

nude mouse heart, liver, lungs, kidneys, and tumors were stained with hematoxylin and eosin (H&E) to examine the pathological changes in various organs and the extent of tumor necrosis. In addition, the sections of the transplanted tumors were subjected to immunohistochemical analysis to evaluate Ki67 expression.

Statistical Analysis

Statistical analysis was performed using GraphPad Prism version 8.0.2 (GraphPad Software, USA). All data are presented as the mean ± standard deviation (SD) from at least three independent experiments. $p < 0.05$ was considered statistically significant.

Results

Optimization and Characterization of the CA7-LP Formulation

To efficiently determine the optimal formulation for CA7-LP, a single-factor study was conducted (Figure 2A). The results showed that both the PS and PDI of CA7-LP initially decreased and then increased as ultrasound intensity increased. As the ultrasound duration was extended, the PS gradually decreased, while the EE initially increased and then decreased, with PDI following the opposite trend. Increasing the CA7 dosage led to a gradual increase in PS, while EE and PDI decreased and increased respectively. Adjusting the lecithin and cholesterol dosages also influenced PS, which initially increased and then decreased, while EE remained relatively stable. The lowest PDI was observed with 125 mg of lecithin and 10 mg of cholesterol. Based on these factors, the initial formulation was determined as follows: ultrasound intensity of 150 W, ultrasound duration of 5 min, CA7 dosage of 5 mg, lecithin dosage of 125 mg, and cholesterol dosage of 10 mg. In addition, sucrose was selected as the lyoprotectant, and the effects of different sucrose concentrations (w/v, 3%, 5%, 10%) on PS and PDI after lyophilization were assessed (Figure 2B). A concentration of 3% sucrose resulted in minimal changes in PS post-lyophilization, making it the preferred lyoprotectant (Figure 2B).

Based on the single-factor findings, three key factors influencing the quality of CA7-LP were selected for optimization: CA7 dosage (X_1), lecithin dosage (X_2), and cholesterol dosage (X_3). The response variables used as evaluation criteria for CA7-LP were PS (Y_1), PDI (Y_2), and EE (Y_3), and BBD was employed. Design Expert 8.0.2 was utilized for polynomial fitting and statistical analysis (Tables S3 and S4). Visually, the high R^2 values (> 0.9) for the fitted equations for PS, PDI, and EE, along with p-values < 0.05, indicated that the models were both effective and predictable (Equation 1, 2, 3). The response surface plots demonstrated how variations in two factors, while holding the third constant, affected PS, PDI, and EE (Figure 2C). Based on the magnitude of the F-values, the ranking of the influences on PS, PDI, and EE was CA7 > Lecithin > Cholesterol (Table S4). Considering the above results, the optimal formulation was determined by Design Expert 8.0.2 as follows: 5.75 mg CA7, 133.41 mg lecithin, and 8.45 mg cholesterol. The PS of the optimized formulation was 92.43 ± 1.52 nm (Table 1, Figure 2D), with a PDI of 0.27 ± 0.01, EE% of 97.79 ± 1.49%, Zeta potential of - 6.69 ± 0.77 mV, and DL% of 3.23 ± 0.20% (Table 1). Transmission electron microscopy confirmed the spherical morphology of CA7-LP (Figure 2E).

$$Y_1 = 94.3227 + 2.9463*X_1 + 2.0296*X_2 + 1.3958*X_3 - 6.3267*X_1*X_2 + 2.3625*X_1*X_3 - 4.0342*X_2*X_3 - 3.8047*X_1^2 - 5.0263*X_2^2 - 8.7072*X_3^2 \left(p = 0.0003, R^2 = 0.9651\right) \quad (1)$$

$$Y_2 = 0.2661 + 0.0071*X_1 + 0.0025*X_2 - 0.0004*X_3 - 0.0031*X_1*X_2 - 0.0023*X_1*X_3 - 0.0055*X_2*X_3 + 0.0091*X_1^2 + 0.0099*X_2^2 + 0.0166*X_3^2 \left(p = 0.0005, R^2 = 0.9573\right) \quad (2)$$

$$Y_3 = 97.4704 - 3.5844*X_1 + 2.9462*X_2 + 0.3701*X_3 + 2.9770*X_1*X_2 + 1.4932*X_1*X_3 - 0.1051*X_2*X_3 - 2.6855*X_1^2 - 0.7891*X_2^2 - 1.7118*X_3^2 \left(p < 0.0001, R^2 = 0.9740\right) \quad (3)$$

CA7-LP Enhances Cellular Uptake of CA7

After treating Hela cells with equimolar doses of CU, CA7, and CA7-LP, green fluorescence was observed within the orange-red cell membrane region in all cases (Figure 3). Compared to CU, CA7 exhibited higher cellular uptake. Notably, CA7-LP showed even stronger fluorescence within the cell nucleus and cytoplasm, indicating that the formulation significantly improves the uptake of CA7.

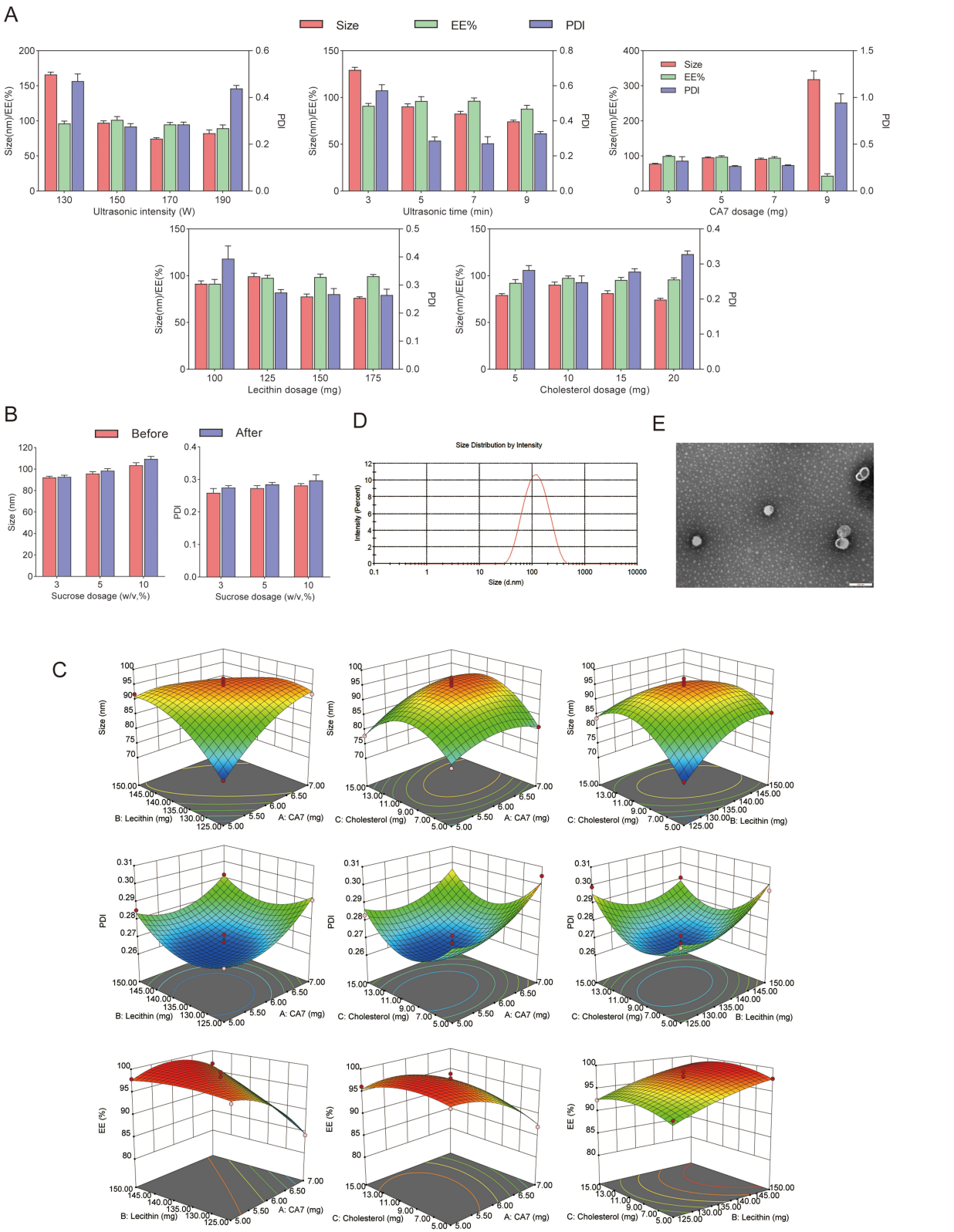

Figure 2 (**A**) The effects of ultrasound intensity, ultrasound time, CA7 dosage, lecithin dosage, and cholesterol dosage on PS, PDI, and EE of CA7-LP. (**B**) The effects of lyophilized protectants on PS and PDI of CA7-LP. (**C**) Two-way interaction contour plots of three factors. (**D**) PS distribution of CA7-LP. (**E**) Morphology of CA7-LP by transmission electron microscopy.

Table 1 Validation Results of CA7-LP

No.	Size	PDI	EE%	Zeta (-mV)	DL (%)
1	90.91	0.26	97.31	−6.83	3.15
2	93.94	0.27	96.54	−5.86	3.47
3	92.45	0.27	99.42	−7.39	3.09
Mean ± SD	92.43 ± 1.52	0.27 ± 0.01	97.79 ± 1.49%	−6.69 ± 0.77	3.23 ± 0.20

CA7-LP Inhibits the Proliferation and Migration of Hela Cells in vitro

By calculating the inhibition rate, as shown in Figure 4A, CA7, CA7-LP, and DDP-INJ all demonstrated strong time- and dose-dependent inhibition of Hela cell growth. In contrast, CU showed minimal variation in its inhibitory effect on Hela cells, and none of the doses surpassed the efficacy of CA7. At 24 h, the maximum inhibition rates for CU and CA7 were 5.77 ± 2.40% and 45.10 ± 9.41%, respectively, with CA7 being 7.8 times more effective than CU. Furthermore, CA7-LP and DDP-INJ exhibited similar IC_{50} values (Figure 4B). Compared to CU and CA7, CA7-LP showed significantly stronger inhibitory effects.

A colony formation assay was used to evaluate the effects of each drug on proliferation of Hela cells. Compared to CU, the number of colony formations was significantly reduced in the CA7, CA7-LP, and DDP groups at various concentrations (Figure 4C and D). Specifically, the colony formation rates induced by CA7-LP (2.5, 5, and 10 μM) were 69.17 ± 6.93%, 17.73 ± 1.40%, and 3.8 ± 0.82%, respectively, all significantly lower than those of CA7 (80.90 ± 10.80%, 57.20 ± 6.50%, 27.20 ± 4.10%). Interestingly, the inhibitory effects of CA7-LP and DDP-INJ were similar overall, which further validated the results of the MTT assay. These findings indicate that CA7 has a superior inhibitory effect on cell proliferation compared to CU, and this effect is further enhanced by CA7-LP.

Wound healing assay was used to investigate the effect of each drug on the migration ability of Hela cells. As shown in Figure 4E and F, the control group showed a migration rate of 61.64 ± 2.38%, indicating a high baseline migration capacity for Hela cells. The CA7 group had a migration rate of 28.51 ± 1.92%, significantly lower than that of CU (42.12 ± 3.06%)

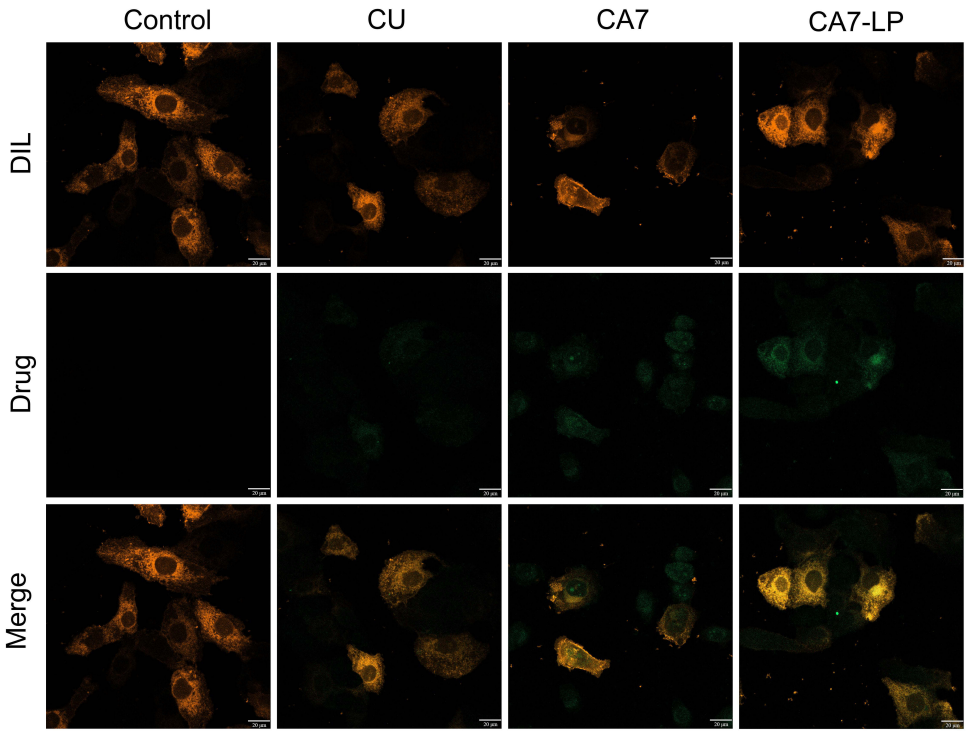

Figure 3 The uptake of CA7-LP by Hela cells.

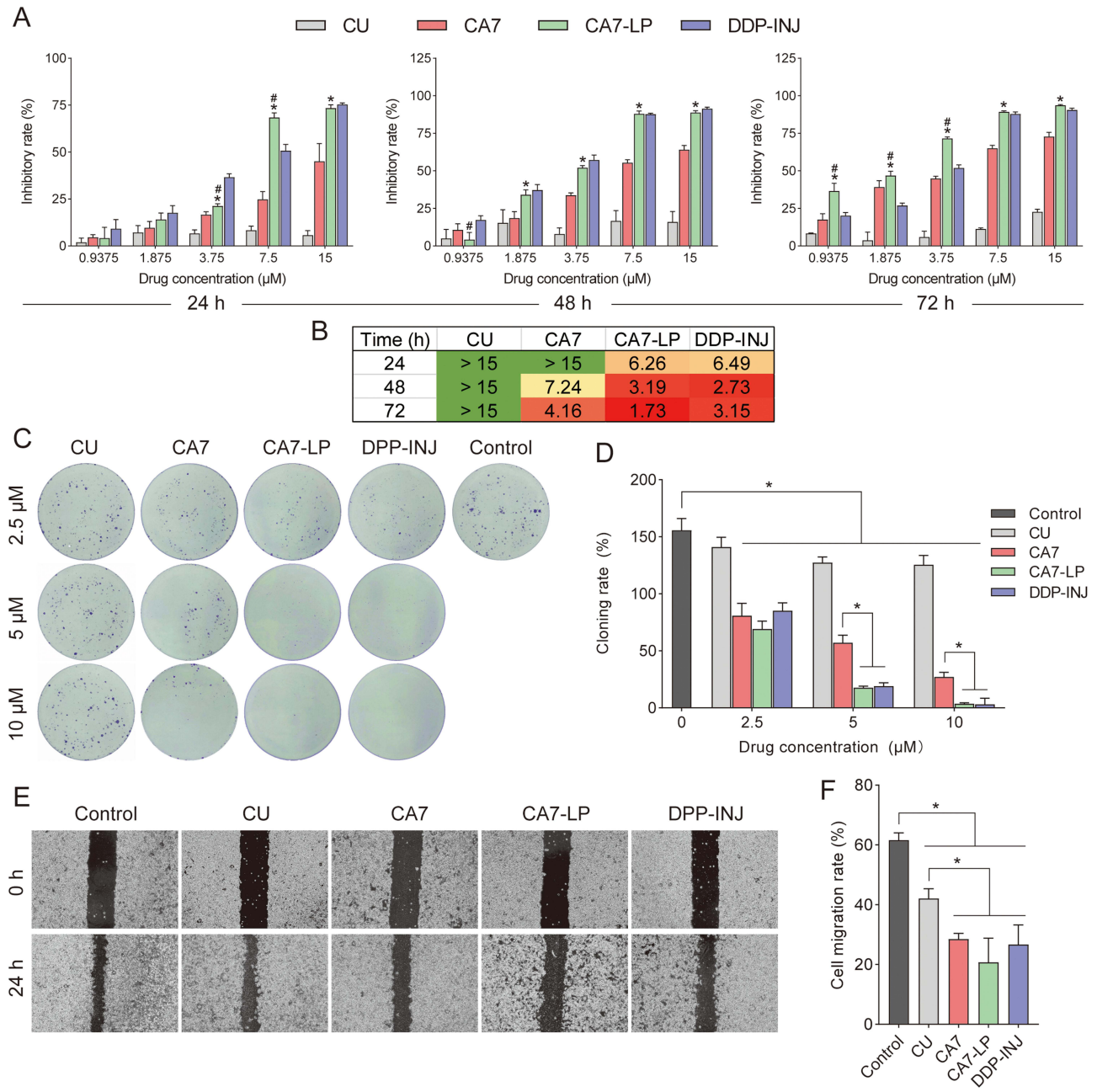

Figure 4 Inhibition of Hela cell activity by CA7-LP. (**A**) The effects of CU, CA7, CA7-LP, and DDP-INJ on Hela cell activity; *$p < 0.05$ vs CA7; #$p < 0.05$ vs DDP-INJ. (**B**) The IC_{50} of CU, CA7, CA7-LP, and DDP-INJ inhibits Hela cell activity. The green color indicates lower toxicity of the drug on Hela cells at the specified time point, while the red color reflects higher toxicity. (**C** and **D**) The effects of CU, CA7, CA7-LP, and DDP-INJ on the proliferation of Hela cells, *$p < 0.05$. (**E** and **F**) The effects of CU, CA7, CA7-LP, and DDP-INJ on the migration of Hela cells, *$p < 0.05$.

($p < 0.05$). Although there was no statistically significant difference in migration inhibition between CA7, CA7-LP, and DDP-INJ ($p > 0.05$), both CA7-LP and DDP-INJ displayed significantly stronger ability to impair migration than CU.

CA7-LP Induces Apoptosis and Cycle Arrest in Hela Cells

Flow cytometry was used to analyze the apoptosis-inducing effects of various drug concentrations on Hela cells. The results showed that early apoptosis rates were higher than late apoptosis rates across all drug concentrations, with total apoptosis rates increasing in a concentration-dependent manner (Figure 5A and B). The total apoptosis rates induced by CA7-LP (2.5, 5, and 10 μM) were 11.93 ± 2.33%, 25.78 ± 2.97%, and 34.11 ± 3.35%, slightly higher than those of DDP-INJ (11.57 ± 1.16%, 23.73 ±

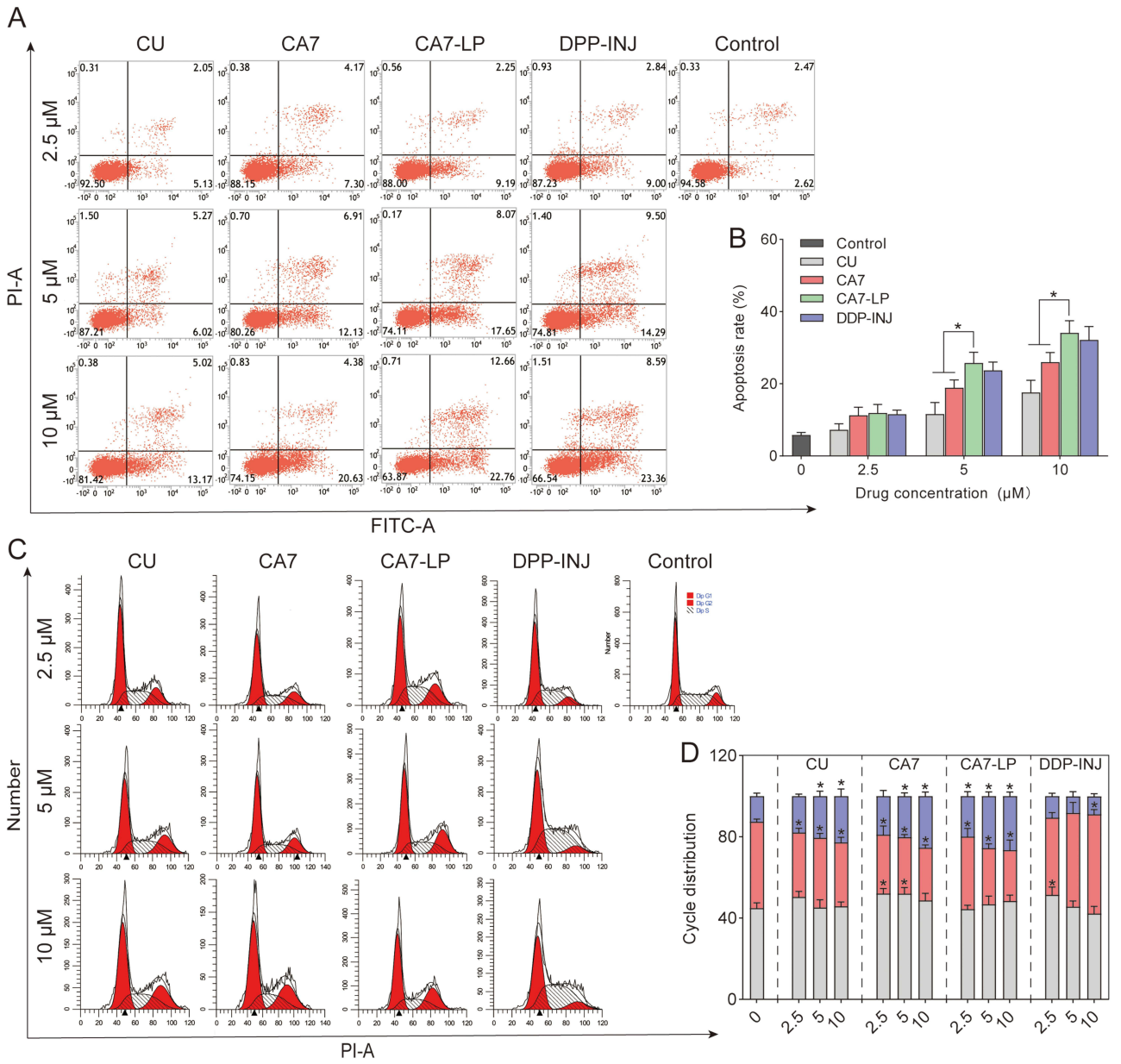

Figure 5 CA7-LP suppressed Hela cells by preventing cell cycle progression and triggering apoptosis. (**A** and **B**) The effects of CU, CA7, CA7-LP, and DDP-INJ on apoptosis induction, *$p < 0.05$. (**C** and **D**) The effects of CU, CA7, CA7-LP, and DDP-INJ on the cell cycle of Hela, *$p < 0.05$ vs Control.

2.30%, 32.17 ± 3.68%). In comparison, CU induced apoptosis rates of 7.29 ± 1.64%, 11.64 ± 3.19%, and 17.60 ± 3.39%, which were lower than those of CA7 (11.26 ± 2.25%, 18.94 ± 2.11%, 26.01 ± 2.69%). In summary, these findings indicate that CA7 more effectively induces apoptosis than CU, while CA7-LP further enhances this effect, surpassing even DDP-INJ in apoptosis induction.

The cell cycle distribution was analyzed using flow cytometry (Figure 5C and D). At concentrations of 2.5, 5, and 10 μM, the proportions of the G2/M phase in the CA7-LP group were 19.88 ± 2.21%, 25.52 ± 2.12%, and 26.50 ± 2.08%, respectively. In the CA7 group, the proportions were 18.94 ± 2.90%, 20.18 ± 1.66%, and 25.32 ± 2.07%. Both CA7-LP and CA7 exhibited similar trends to the CU group (17.84 ± 1.07%, 20.46 ± 2.44%, 22.78 ± 3.60%), inducing G2/M phase arrest of Hela cells in a concentration-dependent manner. In contrast, the DDP group showed an increase in the S phase and a decrease in G2/M phase. In conclusion, these results suggest that CU, CA7, and CA7-LP inhibit Hela cell proliferation partly by inducing G2/M phase cell cycle arrest.

CA7-LP Stability Study

Firstly, the stability of the CA7-LP suspension was evaluated at 25°C and 4°C by monitoring PS, PDI, and EE over time. It was observed that when stored at 25°C, the CA7-LP suspension remained stable for 7 d, with no significant changes in PS, PDI, and EE ($p > 0.05$) (Figure 6A). However, after 15 d, a rapid decrease in EE was observed. In contrast, when stored at 4°C, PS, PDI, and EE remained stable for 15 d ($p > 0.05$) (Figure 6B). These results indicate that the CA7-LP suspension can be stored at room temperature for 7 d, and at 4°C for 15 d, without significant loss of stability.

To facilitate clinical use and storage, CA7-LP was further prepared as a lyophilized powder, and its storage stability at 25°C for 90 days was investigated. As shown in Figure 6C, compared to day 0, there were no significant changes in the PS, PDI, and EE of CA7-LP within 90 d ($p > 0.05$). Therefore, under the aforementioned conditions, the lyophilized powder of CA7-LP can be stored for at least 90 d.

In vitro Release Studies of CA7-LP

The in vitro release profiles of CA7-LP and free CA7 suspension are shown in Figure 6D. The release data were fitted to various models, with the results summarized in Table 2. Among the models, the first-order release model provided the best fit for both free CA7 and CA7-LP. It was observed that the cumulative release of free CA7 remained relatively constant after 8 h, reaching 13.56 ± 2.00% at 24 h (Figure 6D). In contrast, CA7-LP exhibited sustained release, with the cumulative release stabilizing after 10 h and reaching 38.57 ± 3.16% at 24 h (2.84 times higher that of free CA7). Additionally, the release rate constant k_1 for CA7-LP was lower than that of free CA7 (Table 2). Thus, CA7-LP demonstrated a delayed drug release behavior within 24 h.

CA7-LP Has Good Biocompatibility

RBCs typically do not undergo hemolysis in saline, though they can rupture in a hypotonic solution. In this study, RBCs in the negative control group (Group 7) treated with saline showed no hemolysis, while those in the positive control group (Group 8) exhibited complete hemolysis, turning bright red (Figure 6E). While the hemolysis rate increased slightly with higher CA7-LP concentrations, the maximum rate was only 5.29 ± 0.76% (Figure 6F). Moreover, no visible hemolysis was observed, demonstrating the good biocompatibility of CA7-LP.

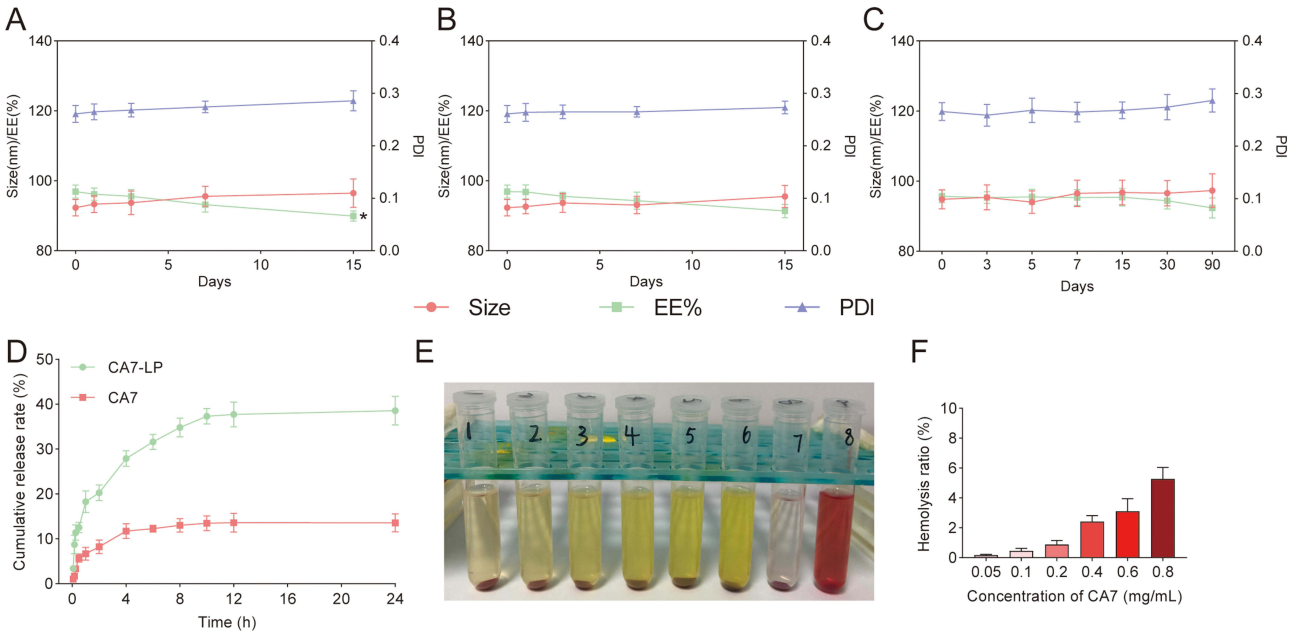

Figure 6 CA7-LP has good stability, release characteristics and biocompatibility. (**A**) Stability of CA7-LP suspension at 25°C, *$p < 0.05$. (**B**) Stability of CA7-LP suspension at 4°C. (**C**) Stability of CA7-LP lyophilized powder at 25°C for 90 d. (**D**) Release curves of CA7-LP in vitro. (**E** and **F**) Biocompatibility Evaluation of CA7-LP.

Table 2 Drug Release Kinetic Parameters and Fitting Coefficients

	Zero-Order R^2	Equation k_0	First-Order R^2	Equation k_1	Higuchi's R^2	Equation k_h
CA7-LP	0.62	1.44	0.90	0.60	0.87	8.15
CA7	0.51	0.51	0.96	0.71	0.79	3.01

Pharmacokinetic Evaluation of CA7-LP

The blood concentrations of free CA7 and CA7-LP over time are shown in Figure 7. Both CA7 and CA7-LP reached their minimum blood drug concentrations at 8 h, which were 0.11 ± 0.03 μg/mL and 0.14 ± 0.05 μg/mL, respectively, and remained undetectable afterward. Pharmacokinetic analysis using DAS 2.1.1 software (Table 3) revealed that CA7-LP significantly improved pharmacokinetic parameters compared to free CA7. Compared to free CA7, CA7-LP exhibited higher AUC (3.58-fold), C_{max} (5.65-fold), and $t_{1/2z}$ (1.2-fold). In conclusion, CA7-LP can enhance the in vivo absorption of CA7 to a certain extent and prolong its duration of action.

CA7-LP Inhibits Xenograft Tumor Growth in vivo

A subcutaneous xenograft model using Hela cells was established to evaluate the anti-CC effects of CA7-LP in vivo. Throughout the experiment, tumor volumes in all groups of nude mice continuously increased over time, initially growing slowly, then accelerating (Figure 8A). Among them, the control group exhibited the fastest tumor growth. In contrast, tumor weights were significantly reduced in the CU, CA7, CA7-LP, and DDP-INJ groups compared to the control (Figure 8C and D). The CA7 group demonstrated a tumor weight of 0.36 ± 0.04 g and an inhibition rate of 47.16 ± 5.70%, which was 1.65 times greater than the CU group (0.49 ± 0.06 g, 28.58 ± 8.04%). Importantly, CA7-LP enhanced the anti-CC efficacy of CA7, showing similar results to DDP-INJ (Figure 8D). Regarding body weight, the mice in the CU, CA7, and CA7-LP groups remained stable throughout the treatment period, with no significant differences compared to the control group ($p > 0.05$) (Figure 8B). However, the DDP-INJ group experienced a notable decrease in body weight, with some mice dying as the number of administrations increased.

Tumor immunohistochemical staining revealed that Ki67-positive cells were lowest in the CA7-LP group, followed by DDP-INJ, CA7, CU, and the control (Figure 8E). H&E staining of the tumors showed varying degrees of necrosis in tumor tissues across all treatment groups (Figure 8F). Furthermore, no pathological changes were observed in the heart and lung tissues of any group (Figure 8G). Tumor cell infiltration was absent in the CA7-LP and DDP groups but present in small amounts in the kidneys and livers of the control, CU, and CA7 groups. In summary, CA7 demonstrated superior anti-CC efficacy compared to CU, while CA7-LP further enhanced this effect.

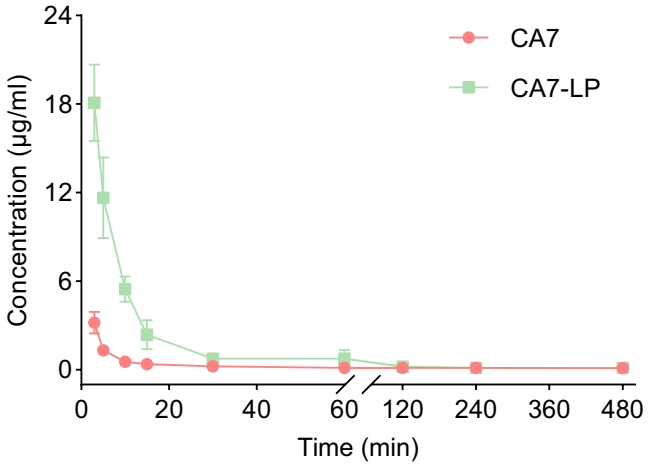

Figure 7 The concentration curves of CA7 and CA7-LP.

Table 3 The Main Pharmacokinetic Parameters of CA7 and CA7-LP

Parameter	Unit	CA7	CA7-LP
$AUC_{(0-t)}$	mg/L×min	80.65	288.43
$MRT_{(0-t)}$	min	177.03	69.65
$t_{1/2z}$	min	149.64	180.27
T_{max}	min	3.00	3.00
V_z	L/kg	118.36	15.97
CL_z	L/min/kg	0.086	0.061
C_{max}	mg/L	3.20	18.09

Discussion

Despite tremendous advancements in the prevention and diagnosis of CC, it remains a substantial challenge to women's health worldwide.[1,4,5] In our previous research, the focus was on improving the anti-CC activity and physicochemical properties of CU, and a CU analog called CA7 was synthesized by our team.[30] LP offer the advantage of improving the pharmacokinetics of existing chemotherapy drugs, coupled with excellent biocompatibility and scalability for large-scale production.[33] In this study, CA7-LP was successfully developed using lecithin and cholesterol as carriers and ultrasound dispersion technology, aiming to enhance the druggability of CA7 through this delivery system.

As widely known, the safety, stability, and drug release efficacy of delivery platforms are significantly influenced by the carrier material. Lecithin and cholesterol utilized in this study are highly safe and biocompatible natural compounds essential for human growth and development.[36] The main phase transition temperature (T_m) is one of the inherent properties of phospholipids. Above T_m, the phospholipid bilayer exhibits higher fluidity and lower alkyl chain order, leading to an unstable system.[37] However, the incorporation of cholesterol, with its rigid sterol ring and the ability to form hydrogen bonds with phospholipids, significantly increases the order of the acyl chains, thereby increasing the stability of LP and reducing drug leakage.[37] Nevertheless, varying the formulation ratios can strongly influence the performance of LP, necessitating optimization. To achieve optimal conditions for CA7-LP formulation, we employed the BBD, which utilizes a quadratic regression equation to predict ideal experimental parameters.[38] Compared to traditional formulation screening, BBD requires fewer experiments, offers greater convenience, and provides higher predictability. Under optimal conditions, the CA7-LP formulation achieved an EE exceeding

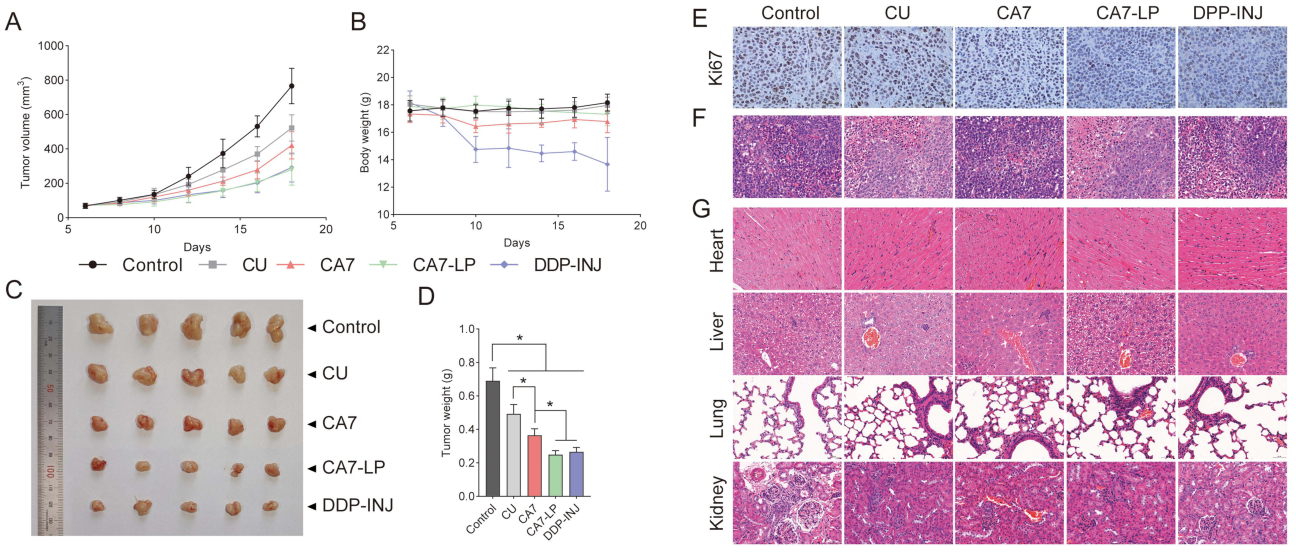

Figure 8 CA7-LP demonstrated favorable anti-CC effects in vivo. (**A**) The curves of tumor volume (n = 5). (**B**) The curves of nude mouse body weight (n = 5). (**C**) Transplanted tumor in nude mice. (**D**) Tumor weight histogram, *$p < 0.05$. (**E**) Immunohistochemical staining of tumors. (**F**) H&E staining of tumors. (**G**) H&E staining of heart, liver, lung and kidney in nude mice.

90%, with small PS and PDI, indicating satisfactory performance. With an approximate PS of 100 nm, CA7-LP is likely to facilitate uptake by the reticuloendothelial system, allowing for passive targeting to tumor sites.[39,40] In vitro release studies showed that a first-order release model best described the release kinetics for both free CA7 and CA7-LP. CA7-LP exhibited a faster initial release rate that gradually decreased over time. This may be attributed to the rapid diffusion of externally available CA7 in the early stages, followed by gradual release from within the LP. Although free CA7 displayed a similar in vitro release profile, its overall release was limited by poor solubility. Importantly, CA7-LP showed improved pharmacokinetic behavior compared to free CA7, suggesting that LP-loaded drugs represent an effective delivery strategy.

Unlimited replicative potential and invasive metastasis are common characteristics of CC and major contributors to patient mortality.[41–43] Previous research has shown that CU can inhibit cancer cell growth, invasion, and migration, as well as induce apoptosis through various pathways, including the Hedgehog/Gli1 pathway,[44] circ-PRKCA/miR-384/ITGB1 pathway,[45] and circ-PLEKHM3/miR-320a/SMG1 pathway.[46] In this study, CA7 demonstrated significantly greater efficacy than CU in inhibiting Hela cell proliferation and migration, inducing apoptosis, and causing cell cycle arrest. Additionally, CA7 demonstrated enhanced in vivo anti-cancer activity compared to CU. Interestingly, the growth inhibition of CC xenografts by CA7 was more pronounced than that observed with tetrahydro-CU.[47] The increased bioavailability, stability, and anti-CC activity of CA7, compared to CU, may be attributed to its unique chemical structure, which features a monocarbonyl carbon chain and a remote 4-hydroxy-3,5-dimethylphenyl moiety. However, further experimental verification is required to confirm this hypothesis. Generally, the pathways for cellular uptake of drug particles are typically endocytosis or fusion.[48] Lipid membranes that resemble cell membrane components are more likely to facilitate the uptake of drugs into cells.[48] CA7-LP exhibited anti-CC activity comparable to that of DDP-INJ, significantly surpassing the effects of CU and CA7 alone. This enhanced efficacy may be attributed to the improved cellular uptake of CA7 facilitated by the LP. Additionally, it is important to note that DDP has been associated with various toxicities, including nephrotoxicity, hepatotoxicity, neurotoxicity, and cardiotoxicity.[49] The findings of this study align with previous research highlighting the toxic effects of DDP; while DDP-INJ demonstrated substantial anti-CC efficacy in vivo, it also led to serious adverse effects in nude mice, with some even dying. Therefore, in clinical practice, careful consideration must be given to balancing therapeutic effectiveness with safety when selecting medications. The promising results of CA7-LP highlight its potential as a more effective and safer alternative for treating CC, warranting further investigation into its clinical applicability.

Conclusion

CA7-LP exhibited an optimal PS distribution, high EE, long-term stability, and favorable drug release characteristics in vitro. Compared to CU or free CA7, CA7-LP enhanced the inhibition of Hela cell proliferation, migration, and cell cycle, as well as increased apoptosis induction. In vivo, CA7-LP demonstrated better pharmacokinetic profiles, comparable anti-CC effects to DDP-INJ, and enhanced safety. Thus, CA7-LP represents a promising new formulation with substantial potential for treating CC.

Abbreviations

CC, Cervical Cancer; LP, liposome; CA7-LP, CA7 liposome; CU, Curcumin; DDP-INJ, Cisplatin Injection; DMEM, Dulbecco's Modified Eagle's Medium; DMSO, Dimethyl Sulfoxide; FBS, Fetal Bovine Serum; EE, Encapsulation Efficiency; DL, Drug Loading; PS, Particle Size; PDI, Polydispersity Index; BBD, Box-Behnken Design; H&E, Hematoxylin and Eosin; SD, Standard Deviation; T_m, Transition Temperature.

Data Sharing Statement

The data generated in this study are available upon request from the corresponding author.

Ethics Approval and Consent to Participate

Animal studies were conducted in accordance with the regulations and guidelines for animal care set forth by Southwest Medical University, and complied with the ARRIVE guidelines. All animal experiments were approved by the Ethics Committee of Southwest Medical University.

Author Contributions

All authors made a significant contribution to the work reported, whether that is in the conception, study design, execution, acquisition of data, analysis and interpretation, or in all these areas; took part in drafting, revising or critically reviewing the article; gave final approval of the version to be published; have agreed on the journal to which the article has been submitted; and agree to be accountable for all aspects of the work.

Funding

This study was supported by the National Natural Science Foundation project of China (No. 82474105), Sichuan Natural Science Foundation Project (No. 2024NSFSC0049, 2024NSFSC0625), Sichuan Science and Technology Program (No. 2022YFS0630, 2022YFS0619), the Key R&D Project of Luzhou-Southwest Medical University (No. 2023LZXNYDHZ002), the Cooperation Projects of Sichuan Credit Pharmaceutical CO., Ltd., Central Nervous System Drug Key Laboratory of Sichuan Province (No. 210027-01SZ, 200017-01SZ, 230007-01SZ, 230008-01SZ), the Chongqing Traditional Chinese Medicine Inheritance and Innovation Team Construction Project "Traditional Chinese Medicine New Drug and Safety Research Inheritance and Innovation Team" (No. 2022-8). Luzhou Science and Technology Plan Project (No. 2023JYJ034, 2023JYJ022, 2022-SYF-85).

Disclosure

The authors report no conflicts of interest in this work.

References

1. Bray F, Laversanne M, Sung H, et al. Global cancer statistics 2022: GLOBOCAN estimates of incidence and mortality worldwide for 36 cancers in 185 countries. *CA Cancer J Clin*. 2024;74(3):229–263. doi:10.3322/caac.21834
2. Xia C, Dong X, Li H, et al. Cancer statistics in China and United States, 2022: profiles, trends, and determinants. *Chin Med J*. 2022;135(5):584–590. doi:10.1097/CM9.0000000000002108
3. Denny L, Kataria I, Huang L, Schmeler KM. Cervical cancer kills 300,000 people a year - here's how to speed up its elimination. *Nature*. 2024;626(7997):30–32. doi:10.1038/d41586-024-00241-2
4. Bosch FX, Lorincz A, Muñoz N, Meijer CJ, Shah KV. The causal relation between human papillomavirus and cervical cancer. *J Clin Pathol*. 2002;55(4):244–265. doi:10.1136/jcp.55.4.244
5. Wilailak S, Kengsakul M, Kehoe S. Worldwide initiatives to eliminate cervical cancer. *Int J Gynaecol Obstet*. 2021;155(Suppl 1):102–106. doi:10.1002/ijgo.13879
6. Cohen PA, Jhingran A, Oaknin A, Denny L. Cervical cancer. *Lancet*. 2019;393(10167):169–182. doi:10.1016/S0140-6736(18)32470-X
7. Loibl S, O'Shaughnessy J, Untch M, et al. Addition of the PARP inhibitor veliparib plus carboplatin or carboplatin alone to standard neoadjuvant chemotherapy in triple-negative breast cancer (BrighTNess): a randomised, Phase 3 trial. *Lancet Oncol*. 2018;19(4):497–509. doi:10.1016/S1470-2045(18)30111-6
8. Nelson KM, Dahlin JL, Bisson J, Graham J, Pauli GF, Walters MA. The essential medicinal chemistry of curcumin. *J Med Chem*. 2017;60(5):1620–1637. doi:10.1021/acs.jmedchem.6b00975
9. Feng T, Wei Y, Lee RJ, Zhao L. Liposomal curcumin and its application in cancer. *Int J Nanomed*. 2017;12:6027–6044. doi:10.2147/IJN.S132434
10. Ataei M, Gumpricht E, Kesharwani P, Jamialahmadi T, Sahebkar A. Recent advances in curcumin-based nanoformulations in diabetes. *J Drug Target*. 2023;31(7):671–684. doi:10.1080/1061186X.2023.2229961
11. Hashemi M, Mirzaei S, Barati M, et al. Curcumin in the treatment of urological cancers: therapeutic targets, challenges and prospects. *Life Sci*. 2022;309:120984. doi:10.1016/j.lfs.2022.120984
12. Yang W, Yang C, Du Y, Wang Q. Colon-targeted release of turmeric nonextractable polyphenols and their anticolitis potential via gut microbiota-dependent alleviation on intestinal barrier dysfunction in mice. *J Agric Food Chem*. 2023;71(30):11627–11641. doi:10.1021/acs.jafc.3c00871
13. Lao CD, Ruffin MT 4th, Normolle D, et al. Dose escalation of a curcuminoid formulation. *BMC Complement Altern Med*. 2006;6:10. doi:10.1186/1472-6882-6-10
14. Zhang X, Zhu L, Wang X, Zhang H, Wang L, Xia L. Basic research on curcumin in cervical cancer: progress and perspectives. *Biomed Pharmacother*. 2023;162:114590. doi:10.1016/j.biopha.2023.114590
15. Einbond LS, Zhou J, Wu HA, et al. A novel cancer preventative botanical mixture, TriCurin, inhibits viral transcripts and the growth of W12 cervical cells harbouring extrachromosomal or integrated HPV16 DNA. *Br J Cancer*. 2021;124(5):901–913. doi:10.1038/s41416-020-01170-3
16. Zhao X, Zhang R, Song Z, et al. Curcumin suppressed the proliferation and apoptosis of HPV-positive cervical cancer cells by directly targeting the E6 protein. *Phytother Res*. 2023;38:4967—4981.
17. Arabnezhad L, Mohammadifard M, Rahmani L, Majidi Z, Ferns GA, Bahrami A. Effects of curcumin supplementation on vitamin D levels in women with premenstrual syndrome and dysmenorrhea: a randomized controlled study. *BMC Complement Med Ther*. 2022;22(1):19. doi:10.1186/s12906-022-03515-2
18. Han H, Alsayed AMM, Wang Y, et al. Discoveryβ of clocitral-derived mono-carbonyl curcumin analogs as anti-hepatocellular carcinoma agents via suppression of MAPK signaling pathway. *Bioorg Chem*. 2023;132:106358. doi:10.1016/j.bioorg.2023.106358

19. Zhao JA, Nie W, Dong L, Liu W, Wei W. A curcumin analog GL63 inhibits the malignant behaviors of hepatocellular carcinoma by inactivating the JAK2/STAT3 signaling pathway via the circular RNA zinc finger protein 83/microRNA-324-5p/cyclin-dependent kinase 16 axis. *J Gastroenterol Hepatol*. 2021;36(10):2967–2977. doi:10.1111/jgh.15545
20. Zhao S, Pi C, Ye Y, Zhao L, Wei Y. Recent advances of analogues of curcumin for treatment of cancer. *Eur J Med Chem*. 2019;180:524–535. doi:10.1016/j.ejmech.2019.07.034
21. Tomeh MA, Hadianamrei R, Zhao X. A review of curcumin and its derivatives as anticancer agents. *Int J Mol Sci*. 2019;20(5):1033. doi:10.3390/ijms20051033
22. Razali NSC, Lam KW, Rajab NF, A Jamal AR, Kamaluddin NF, Chan KM. Curcumin piperidone derivatives induce anti-proliferative and anti-migratory effects in LN-18 human glioblastoma cells. *Sci Rep*. 2022;12(1):13131. doi:10.1038/s41598-022-16274-4
23. Wei T, Zheng Z, Wei X, et al. Rational design, synthesis, and pharmacological characterisation of dicarbonyl curcuminoid analogues with improved stability against lung cancer via ROS and ER stress mediated cell apoptosis and pyroptosis. *J Enzyme Inhib Med Chem*. 2022;37(1):2357–2369. doi:10.1080/14756366.2022.2116015
24. Ghosh H, Bhattacharyya S, Schobert R, Dandawate P, Biersack B. Fluorinated and N-acryloyl-modified 3,5-Di[(E)-benzylidene]piperidin-4-one curcuminoids for the treatment of pancreatic carcinoma. *Pharmaceutics*. 2023;15(7):1921. doi:10.3390/pharmaceutics15071921
25. Shen H, Shen J, Pan H, et al. Curcumin analog B14 has high bioavailability and enhances the effect of anti-breast cancer cells in vitro and in vivo. *Cancer Sci*. 2021;112(2):815–827. doi:10.1111/cas.14770
26. Duan Y, Chen HL, Ling M, et al. The curcumin analog EF24 inhibits proliferation and invasion of triple-negative breast cancer cells by targeting the long noncoding RNA HCG11/Sp1 axis. *Mol Cell Biol*. 2022;42(1):e0016321. doi:10.1128/MCB.00163-21
27. Li J, Wang SH, Liu YT, Zhang Q, Zhou GZ. Inhibition of autophagic flux by the curcumin analog EF-24 and its antiproliferative effect on MCF-7 cancer cells. *J Biochem Mol Toxicol*. 2023;37(4):e23307. doi:10.1002/jbt.23307
28. Doan NQH, Nguyen NTK, Duong VB, et al. Synthesis, biological evaluation, and molecular modeling studies of 1-Aryl-1H-pyrazole-fused curcumin analogues as anticancer agents. *ACS Omega*. 2022;7(38):33963–33984. doi:10.1021/acsomega.2c02933
29. Rahim NFC, Hussin Y, Aziz MNM, et al. Cytotoxicity and apoptosis effects of curcumin analogue (2E,6E)-2,6-Bis(2,3-dimethoxybenzylidine) cyclohexanone (DMCH) on human colon cancer cells HT29 and SW620 in vitro. *Molecules*. 2021;26(5):1261. doi:10.3390/molecules26051261
30. Zhao L, Wei YM, Pi CH, et al. A monocarbonyl-like curcumin analog and its preparation method and application. CN Patent ZL202110585306.8; 2022.
31. Barenholz Y. Doxil®–The first FDA-approved nano-drug: lessons learned. *J Control Release*. 2012;160(2):117–134. doi:10.1016/j.jconrel.2012.03.020
32. Bulbake U, Doppalapudi S, Kommineni N, Khan W. Liposomal formulations in clinical use: an updated review. *Pharmaceutics*. 2017;9(2):12. doi:10.3390/pharmaceutics9020012
33. Taléns-Visconti R, Díez-Sales O, de Julián-Ortiz JV, Nácher A. Nanoliposomes in cancer therapy: marketed products and current clinical trials. *Int J Mol Sci*. 2022;23(8):4249. doi:10.3390/ijms23084249
34. Luo H, Lu L, Liu N, Li Q, Yang X, Zhang Z. Curcumin loaded sub-30 nm targeting therapeutic lipid nanoparticles for synergistically blocking nasopharyngeal cancer growth and metastasis. *J Nanobiotechnology*. 2021;19(1):224. doi:10.1186/s12951-021-00966-6
35. Shariare MH, Khan MA, Al-Masum A, Khan JH, Uddin J, Kazi M. Development of stable liposomal drug delivery system of thymoquinone and its in vitro anticancer studies using breast cancer and cervical cancer cell lines. *Molecules*. 2022;27(19):6744. doi:10.3390/molecules27196744
36. Zeisel SH, da Costa KA. Choline: an essential nutrient for public health. *Nutr Rev*. 2009;67(11):615–623. doi:10.1111/j.1753-4887.2009.00246.x
37. Cheng CY, Lai YF, Hsieh YL, Wu CH, Chiu CC, Yang YM. Divergent effects of cholesterol on the structure and fluidity of liposome and catanionic vesicle membranes. *FEBS Lett*. 2022;596(14):1827–1838. doi:10.1002/1873-3468.14375
38. Abla KK, Mneimneh AT, Allam AN, Mehanna MM. Application of box-behnken design in the preparation, optimization, and in-vivo pharmacokinetic evaluation of oral tadalafil-loaded niosomal film. *Pharmaceutics*. 2023;15(1):173. doi:10.3390/pharmaceutics15010173
39. Golombek SK, May JN, Theek B, et al. Tumor targeting via EPR: strategies to enhance patient responses. *Adv Drug Deliv Rev*. 2018;130:17–38. doi:10.1016/j.addr.2018.07.007
40. Lundy DJ, Lee KJ, Peng IC, et al. Inducing a transient increase in blood-brain barrier permeability for improved liposomal drug therapy of glioblastoma multiforme. *ACS Nano*. 2019;13(1):97–113. doi:10.1021/acsnano.8b03785
41. Suran M. why us cervical cancer survival rates haven't improved for decades. *JAMA*. 2022;327(20):1943–1945. doi:10.1001/jama.2022.4681
42. Zhong G, Zhao Q, Chen Z, Yao T. TGF-β signaling promotes cervical cancer metastasis via CDR1as. *Mol Cancer*. 2023;22(1):66. doi:10.1186/s12943-023-01743-9
43. Wenzel HHB, Olthof EP, Bekkers RLM, et al. Primary or adjuvant chemoradiotherapy for cervical cancer with intraoperative lymph node metastasis - A review. *Cancer Treat Rev*. 2022;102:102311. doi:10.1016/j.ctrv.2021.102311
44. Li M, Guo T, Lin J, et al. Curcumin inhibits the invasion and metastasis of triple negative breast cancer via Hedgehog/Gli1 signaling pathway. *J Ethnopharmacol*. 2023;283:114689. doi:10.1016/j.jep.2021.114689
45. Xu X, Zhang X, Zhang Y, Wang Z. Curcumin suppresses the malignancy of non-small cell lung cancer by modulating the circ-PRKCA/miR-384/ITGB1 pathway. *Biomed Pharmacother*. 2021;138:111439. doi:10.1016/j.biopha.2021.111439
46. Sun S, Fang H. Curcumin inhibits ovarian cancer progression by regulating circ-PLEKHM3/miR-320a/SMG1 axis. *J Ovarian Res*. 2021;14(1):158. doi:10.1186/s13048-021-00916-8
47. Yoysungnoen B, Bhattarakosol P, Patumraj S, Changtam C. Effects of tetrahydrocurcumin on hypoxia-inducible factor-1α and vascular endothelial growth factor expression in cervical cancer cell-induced angiogenesis in nude mice. *Biomed Res Int*. 2015;2015:391748. doi:10.1155/2015/391748
48. Gandek TB, van der Koog L, Nagelkerke A. A comparison of cellular uptake mechanisms, delivery efficacy, and intracellular fate between liposomes and extracellular vesicles. *Adv Healthc Mater*. 2023;12(25):e2300319. doi:10.1002/adhm.202300319
49. Dasari S, Njiki S, Mbemi A, Yedjou CG, Tchounwou PB. Pharmacological effects of cisplatin combination with natural products in cancer chemotherapy. *Int J Mol Sci*. 2022;23(3):1532. doi:10.3390/ijms23031532